JEE Journal of Ecological Engineering

Journal of Ecological Engineering 2022, 23(6), 30–42
https://doi.org/10.12911/22998993/147806
ISSN 2299–8993, License CC-BY 4.0

Received: 2022.03.10
Accepted: 2022.04.12
Published: 2022.04.20

Simultaneous Adsorption of Ternary Antibiotics (Levofloxacin, Meropenem, and Tetracycline) by SunFlower Husk Coated with Copper Oxide Nanoparticles

Mohammed A. Ibrahim[1], Mohammed Ali A. Shaban[1], Yaseen Rashid Hasan[2], Mohanad J. M-Ridha[3], Haitham A. Hussein[1], Khalid M. Abed[4,5], Sabah J. Mohammed[3], Mohd Hafizuddin Muhamad[6], Hassimi Abu Hasan[6,7*]

[1] Department of Civil Enginering, College of Engineering, Al-Nahrain University, Baghdad, Iraq
[2] Reconstruction and Projects Directorate, Ministry of Higher Education and Scientific Research, Baghdad, Iraq
[3] Department of Environmental Engineering, College of Engineering, University of Baghdad, Iraq
[4] Department of Chemical Engineering, College of Engineering, University of Baghdad, Iraq
[5] Department of Chemical Engineering, Faculty of Engineering, Universiti Malaya, Kuala Lumpur, Malaysia
[6] Department of Chemical and Process Engineering, Faculty of Engineering and Built Environment, Universiti Kebangsaan Malaysia, 43600 UKM Bangi, Selangor, Malaysia
[7] Research Centre for Sustainable Process Technology (CESPRO), Faculty of Engineering and Built Environment, Universiti Kebangsaan Malaysia, 43600 UKM Bangi, Selangor, Malaysia
* Corresponding author's e-mail: hassimi@ukm.edu.my

ABSTRACT

In this study, a new adsorbent derived from sunflower husk powder and coated in CuO nanoparticles (CSFH) was investigated to evaluate the simultaneous adsorption of Levofloxacin (LEV), Meropenem (MER), and Tetracycline (TEC) from an aqueous solution. Significant improvements in the adsorption capacity of the sunflower husk were identified after the powder particles had been coated in CuO nanoparticles. Kinetic data were correlated using a pseudo-second-order model, and was successful for the three antibiotics. Moreover, high compatibility was identified between the LEV, MER, and TEC, isotherm data, and the Langmuir model, which produced a better fit to suit the isotherm curves. In addition, the spontaneous and exothermic nature of the adsorption process was crucial for transforming the three antibiotics into CSFH. The greatest CSFH adsorption capacity was in MER (131.83 mg/g), followed by TEC (96.95 mg/g), and LEV (62.24 mg/g). These findings thus indicate that CSFH is one of the most effective and efficient adsorbents to use for eliminating wastewater contaminated with antibiotic residue.

Keywords: adsorption, antibiotics, neural network, wastewater, sustainable process.

INTRODUCTION

Recently, the presence of antibiotics in aquatic environments has emerged as a prominent environmental problem. This can have major negative impacts on human and environmental health (Mohammed et al., 2021). In fact, antibiotics have been recently classified as new water contaminants that pose significant risks to the environment due to their toxic nature. As well as impacting human and animal health, antibiotics can also have a substantial long-term impact on ecological sustainability (Michael et al., 2013; Pouretedal and Sadegh, 2014). Releasing antibiotics into the environment increases the levels of antibiotic resistant bacteria, which makes the treatment process more challenging. Conventional wastewater treatment systems can be ineffective in removing prescription antibiotics. As a result, there is a rising need to develop more effective solutions to treat these pollutants (Ternes et al., 2004).

Numerous researchers have investigated methods of removing different antibiotics from wastewater. Some studies (Mohseni-Bandpi et al., 2016) have focused on the removal of cephalexin, whereas others have investigated amoxicillin, ciprofloxacin (Danalıoğlu et al., 2017; Sun et al., 2016; Wu et al., 2010), alkaloids (Abed et al., 2014; Abed et al., 2015), pelletierine (Al-Hemiri et al., 2012), levofloxacin (Mohammed and Mohammed-Ridha, 2021), combined levofloxacin and ciprofloxacin (Mohammed et al., 2021), metronidazole (Ahmed et al., 2013; Teixeira et al., 2019), norfloxacin (Yang et al., 2012), naproxen (Attia et al., 2013), and ibuprofen (Fukahori and Fujiwara, 2014).

Levofloxacin (LEV), meropenem (MER), and tetracycline (TEC) are very common antibiotics used worldwide to treat different bacterial diseases. Thus, the effects that these antibiotics have when released into the environment have been explored in great depth. LEV is a relatively new and more advanced antibiotic than other fluoroquinolones (FQs). FQs are a wide-range class of synthetic antibiotics that function by inhibiting the growth of the bacterial DNA gyrase enzyme needed by bacteria to replicate. This antibiotic is highly resistant to traditional biological oxidation and normally manages to escape intact from wastewater treatment plants (WWTPs) (Mahmoud et al., 2020). LEV can inhibit both Gram-positive and Gram-negative bacteria. For this reason, it can be used to treat a wide variety of infections such as skin and soft tissues infections, obstetric, genitourinary, and gynaecological infections (Al-Jabari et al., 2019).

On the other hand, MER is a wide-ranging injectable β-lactam antibiotic typically administered to treat serious bacterial infections such as those that affect the lower respiratory tract, as well as intraabdominal, urinary tract, obstetric/gynaecological, meningitis, cystic fibrosis and in-febrile neutropenia infections (Elragehy et al., 2008; M-Ridha et al., 2020; Shaban et al., 2020; Wang et al., 2020). TEC is the second most commonly used antibiotic worldwide used to effectively treat a wide range of infections (Ersan et al., 2015). This antibiotic has been recently detected in soils, groundwater, and surface waters (Song et al., 2019). The chemical structure of TEC antibiotics facilitates the cation exchange between the soil and sediment clay components, playing a significant role in determining the sorption mechanisms of these antibiotics (Figueroa et al., 2004). As TEC molecules tend to be neutral or negatively charged in environmental water and thus traditional methods for removing antibiotics from wastewater (such as sedimentation, sand filtration, flocculation, and coagulation), are not very effective for eliminating tetracycline (Soori et al., 2016).

Adsorption is an effective and appealing technique that can be used to eliminate contaminants from water, with simple process management and minimal operating costs (Inyang et al., 2014; Yi et al., 2015). Various materials such as resins, activated carbon, and carbon nano-materials have been used to absorb several antibiotics and effectively remove them from water (Chen et al., 2015; Tian et al., 2013a, 2013b). Recently, more studies have been performed in order to find ways to improve the adsorption capacity of natural waste material and create highly efficient adsorbents. Coating the adsorbent surface with nanoparticles was first applied by Gupta and Saleh (2013), and the efficiency was high as it can enhance the mechanical strength, surface area, and adsorption capacity of the adsorbent.

Gold, alumina, zinc oxide, iron oxide, stannous oxide, titanium oxide, copper oxide, and a number of alloys have been used to create nanoparticle adsorbents for wastewater treatment. Pure nanoparticles are expensive and generally unsuitable due to their strong tendency to agglomerate, resulting in significant reactivity loss and a drop in pressure in traditional treatment systems (Shi et al., 2011). Moreover, advanced filtration technology is required to remove them from the aqueous phase (Shi et al., 2011; Tian et al., 2013a). Using natural adsorbents coated with nanoparticles is thus a more viable option because it overcomes the drawbacks of using nanomaterials in isolation. Additionally, this enhances the effectiveness of the main adsorbents in removing impurities from various sources (Mohseni-Bandpi et al., 2016).

Therefore the aims of this study was to investigate the potential of simultaneous adsorption of LEV, MER, and TEC using sunflower husk coated with copper oxide nanoparticles (CSFH). The synthesised CSFH was chareterised under X-ray diffractometer (XRD), scanning electron microscopy (SEM), Fourier transform infra-red (FTIR), and Brunauer–Emmett–Teller (BET). The adsorption capabilities were investigated by maniputing the initial concentration, temperature, contact time, and pH. The thermodynamics and kinetics of the CSFH adsorpion were also determined for each antibiotics. In addition, artificial neural network (ANN) was developed to predict the adsorption of the antibiotics.

MATERIALS AND METHODS

Ternary antibiotics preparation

The following chemicals used in the present investigation were supplied by the original manufacturer (Merck, Germany): powdered LEV hemihydrate ($C_{36}H_{42}F_2N_6O_9$), MER ($C_{17}H_{25}N_3O_5$ S), TEC hydrochloride ($C_{22}H_{24}O_8N_2$.HCl). The stock solutions were prepared before the start of each experiment with 0.1 g of powdered antibiotic (LEV, MER, and TEC) dissolved in 1 L of deionised water in order to produce 100 mg/L ternary antibiotics concentrations. Subsequently, the solutions were stirred for one hour to produce a homogenous ternary solution.

Synthesis of CSFH

A sunflower husk was washed with deionised water and dried in an oven at 105 °C. It was then left overnight, ground, and sieved (mesh No. 200). The remaining powder was collected and placed in a container. Additionally, 300 g of 99% pure CuO nanoparticles (Nanostructured and Amorphous Materials Inc., Houston, TX, USA) were purchased. The collected CuO nanoparticles were then subjected to a sonolysis process for 30 min to ensure that they were dispersed thoroughly in the acetone. Subsequently, the powdered sunflower husks was placed in the CuO nanoparticles solution at a ratio of 5:1 (g/g) and stirred until a homogenous mixture was produced. The liquid was then decanted, which left CSFH precipitates, filtered, and dried in an oven at 60 °C. Lastly, when completely dry, the CSFH was placed in flasks prior to use.

Characterisation of CSFH

Characterisation of the adsorbent was conducted with raw SFH and CSFH. An X-ray diffractometer (XRD; Philips-Magix Pro MPD, Netherlands) was employed to identify the CSFH's crystalline structure. The patterns fell within a range of 2θ, varying between 5° and 60°, with a step width of 0.02° and scan rate of 1° per sec. An SEM (TESCAN-Vega3, Czech Republic) was also used to identify the surface morphology of the CSFH. EDS analysis was then performed to determine the elemental composition. A Shimadzu FTIR spectroscopy was employed to identify the functional groups present on the CSFH. A BET analysis was performed to examine the specific surface area of the SFH and CSFH. Furthermore, the pH of the CSFH's zero points of charge (pHzpc) was calculated using the method outlined by Mohseni-Bandpi et al. (2016). This test was required to determine the type of CSFH surface charge in relation to the pH of the solution.

Adsorption experiments

The adsorption tests were carried out in a batch-ternary system. Mixtures containing different concentrations of antibiotics solution (5, 25, 50, and 75 mg/L) were placed in 25 mL conical flasks, and agitated at 200 rpm with CSFH adsorbent (0.1 g/100 mL antibiotic solution) using an orbital shaker (LSI-3016R; Labtech, Korea). The sorption effects were measured with different pollutant concentrations at various points in time. Moreover, the influence of temperature on sorption was investigated at temperatures ranging from 20–40 °C. At contact time of 5 to 90 min, 10 mL sample was collected and centrifuged (PLC-03-GEMMY, Taiwan) at 3000 rpm for 5 minutes. An ultraviolet-visible spectrophotometer (UV/VIS-T80-PG, UK) was then used to measure the remaining antibiotics concentration. The maximum adsorption wavelength set on the spectrophotometer was 296 nm. The impact of the adsorbate dosage and initial pH (range 3–9) on the CSFH pollutant removal capability was also investigated. The following equations (1) and (2) (Mohseni-Bandpi et al., 2016; Shaban et al., 2020) were used to compute the ternary antibiotics removal efficiency (percentage) and equilibrium adsorption capacity (qe, mg/g):

$$R(\%) = \frac{(C_o - C_e)}{c_o} \times 100 \quad (1)$$

$$\mathrm{q_e} = \frac{(C_o - C_e)V}{m} \quad (2)$$

where: C_o – represents the initial concentrations of ternary antibiotics;
C_e – represents the equilibrium concentrations (mg/L);
V – is the volume of used solution (L);
M – representing the mass of adsorbent applied (g).

RESULTS AND DISCUSSION

Characterisation of the SFH and CSFH

Figure 1 shows the SEM micrographs of the SFH and CSFH before and after simultaneous adsorption of LEV, MER, and TEC molecules. Coating the nanoparticles in CuO radically alters the morphological features of the SFH (Figures 1a and 1b). The SEM images of the CSFH suggests that the adsorbent has a coarse surface and is made up of various non-uniform and separated aggregates. A number of large ravines and long grooves can be seen in the outer wall of the CSFH particles. The presence of a large surface area and active sites for the adsorbtion of adsorbate molecules are significant benefits. When comparing Figure 1b with the SEM image of the CSFH after adsorption (Figure 1c), it is evident that the morphological features of the CSFH are substantially changed during the simultaneous antibiotic adsorption process. The CSFH surface appears to become smoother, whilst various pre-separated aggregates have coalesced owing to the adsorption of the three antibiotics on active CSFH sites.

By collecting the EDS spectrums of the CSFH prior to and after adsorption reactions with the three antibiotics, the elemental composition of the CSFH could be ascertained. The elements C and Ca are clearly visible in the EDS spectra of the CSFH before adsorption. Furthermore, the high mass ratio of Cu and O elements indicate that the interaction between sunflower husk and the CuO nanoparticles has been effective. After the reaction, the Cu is found in the EDS spectrum of the CSFH. This shows that CuO nanoparticles on the CSFH surface are stable following adsorption. XRD analysis performed on the SFH and CSFH clearly show that carbonate is the dominant material in the SFH's crystallographic structure, which occur naturally in the SFH. Moreover, small traces of these elements can be detected in the PS XRD pattern. The analysis of the XRD CSFH spectra reveal additional peaks once SFH is coated with CuO nanoparticles.

FTIR analysis was performed on the raw SFH sample is shown in Figure 2a. This analysis revealed that bands of aliphatic C-H ranging from 3000–2800 cm^{-1} and C = O bonding in the 1745–1725 cm^{-1} range indicate the presence of fats in this agricultural material (Mohammed et al., 2020). Figure 2a shows three functional groups in the SFH FTIR spectrum. The broad band identified at 3788.19 and 3410 cm^{-1} can be assigned to the O-H amide group and O-H alcohol bond group. On the other hand, the band identified at 2937.59 cm^{-1} appears to be an Alkanes C-H bond stretching functional group. The two bands identified at 1627.9 and 1406.1 cm^{-1} appear to have polymer chain bonds that are characteristic of allyl alcohol, whilst they can also be assigned to the vinyl-CH2 group based on their C=C stretching vibrations (Dostert et al., 2016). Lastly, the bond at 1056 cm^{-1} contains a rans-wag vibration and features characteristic of the C=O = aldehyde group and the C=C = vinyl group (Dostert et al., 2016).

Clear changes can be seen in the CSFH FTIR bands (Figure 4b) compared to the SFH spectrum, with the new values being as follows: 2914.4, 2341.5, 1641.4, 1409.9, and 472.56 cm^{-1}. This

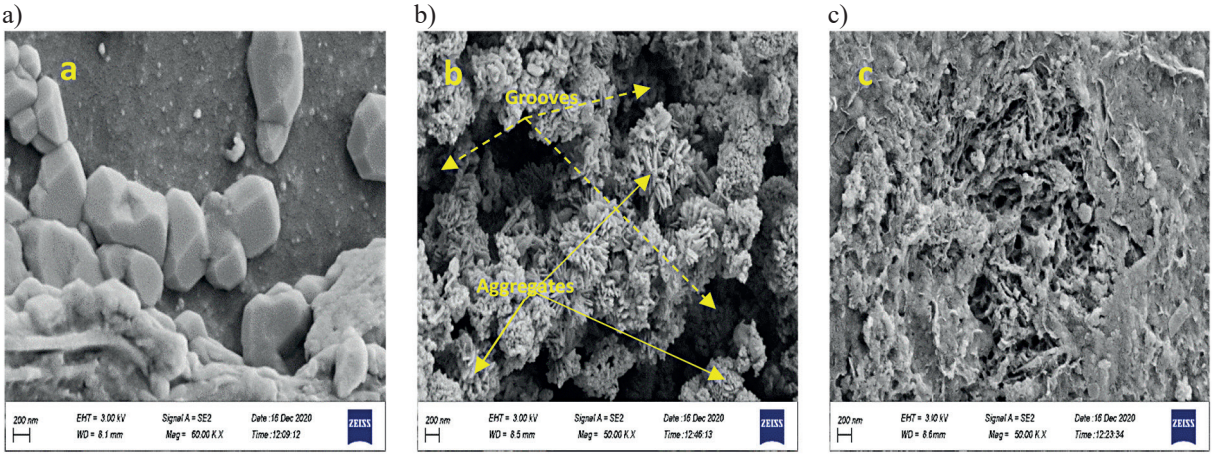

Figure 1. SEM micrographs of SFH(a) and CSFH before (b), and after (c) simultaneous adsorption of LEV, MER, and TEC. SEM, scanning electron microscopy; SFM, sunflower husk; CSFH, CuO coated SFM; LEV, Levofloxacin; MER, Meropenem; TEC, Tetracycline

change is likely caused by the interactions between raw SFH and the CuO nanoparticles in the coating material. Moreover, the band detected at 1641.4 cm^{-1} has similar vibration stretching patterns to the carbonyl group or carboxylic bonds (Dostert et al., 2016). This is most likely caused by the reactive carbon-containing plasma groups that are activated throughout the synthesis of CuO nanoparticles (Ramani et al., 2015). The FTIR spectra for CSFH after the adsorption procedure of three medicinal items are shown in Figure 2c. When comparing the FTIR CSFH spectrum before (Figure 2b) and after (Figure 2c) adsorption, there has been a slight increase in the intensity of the band at 3405 (Figure 2b). As described by Mohammed et al. (2020), the pollutant molecules' overlap the –OH and –NH2 stretching vibrations. Further, the bands identified at 1631.78, 1247.94, 1107.32, and 584.43 cm^{-1} have shifted, implying that these functional groups are involved in pollutant molecule sorption. The results also indicate that the band corresponding to CuO (<1000 cm^{-1}) is still present in the CSFH FTIR spectrum once adsorption has taken place. Therefore, CuO nanoparticles remain attached to the SFH surface throughout the adsorption process.

Adsorption of ternary antibiotics

Effect of pH and contact time

Adsorbate molecules, however, can have different surface charges at different pH values, which ultimately has a significant impact on their

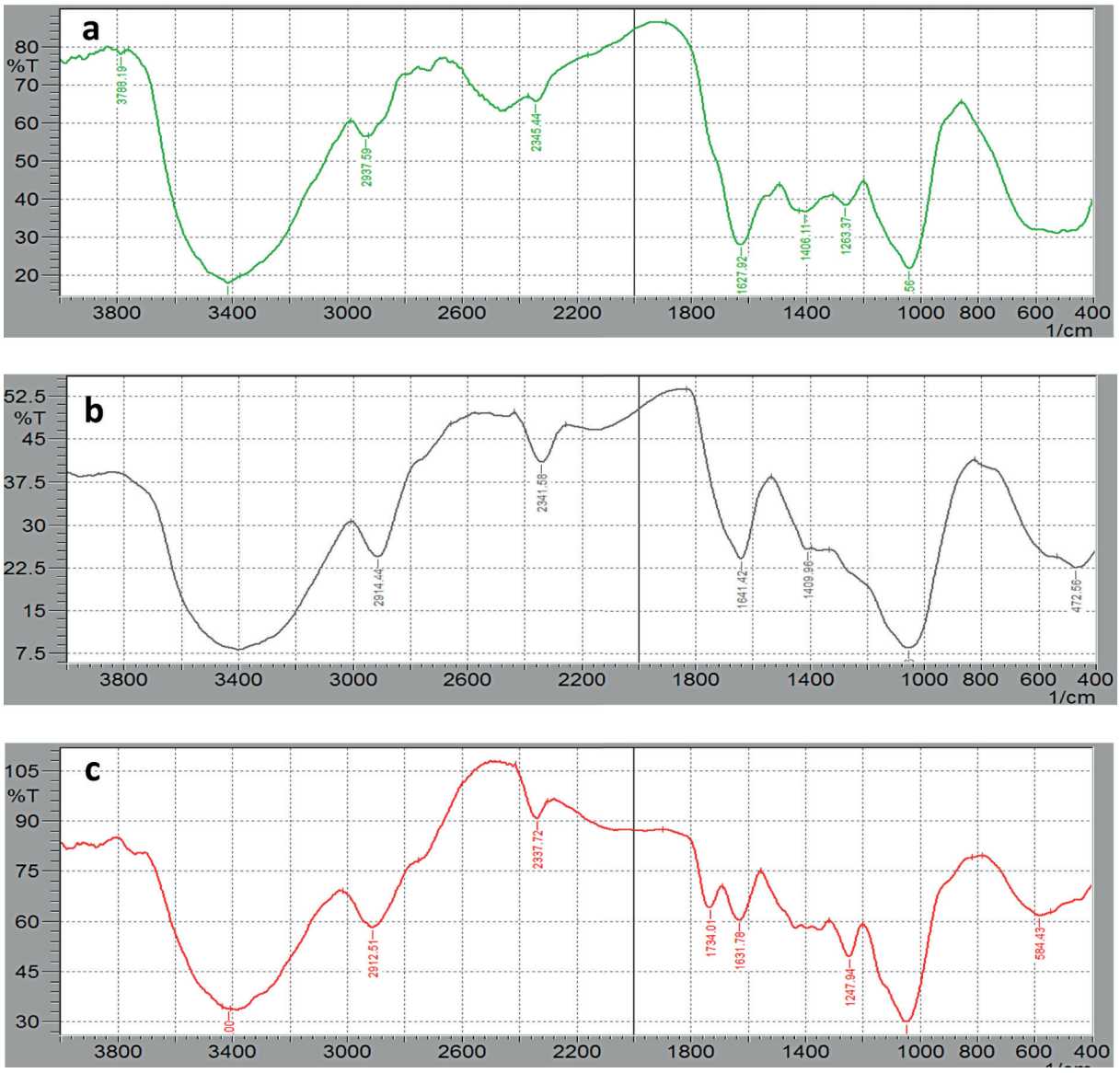

Figure 2. FT-IR analysis of SFH (a), and CSFH before (b), and after (c) simultaneous adsorption of LEV, MER, and TEC molecules. FT-IR, Fourier-transform infrared

adherence to adsorbent particles. Figure 3 shows the variation in removal of LEV, MER, and TEC as a function of pH. The amount of each antibiotic adsorbed onto the CSFH in the ternary system increases as the pH rises from 4 to 7, and then decreases as the pH level rises. The electrostatic interactions that take place between antibiotic molecules and the CSFH surface can explain this adsorption. The analysis showed that the pHpzc of the CSFH was 6.5. Moreover, the surface of a CuO nanoparticle often contains neutral-charged hydroxyl (OH) groups, although these can differ depending on the pH level.

The H^+ ions detach from the particle surface at pH > pHpzc due to the negative charging of CuO with partially bonded oxygen atoms (CuO). On the other hand, pH < pHpzc, H^+ are drawn to the particle surface where they bond with OH^- groups,

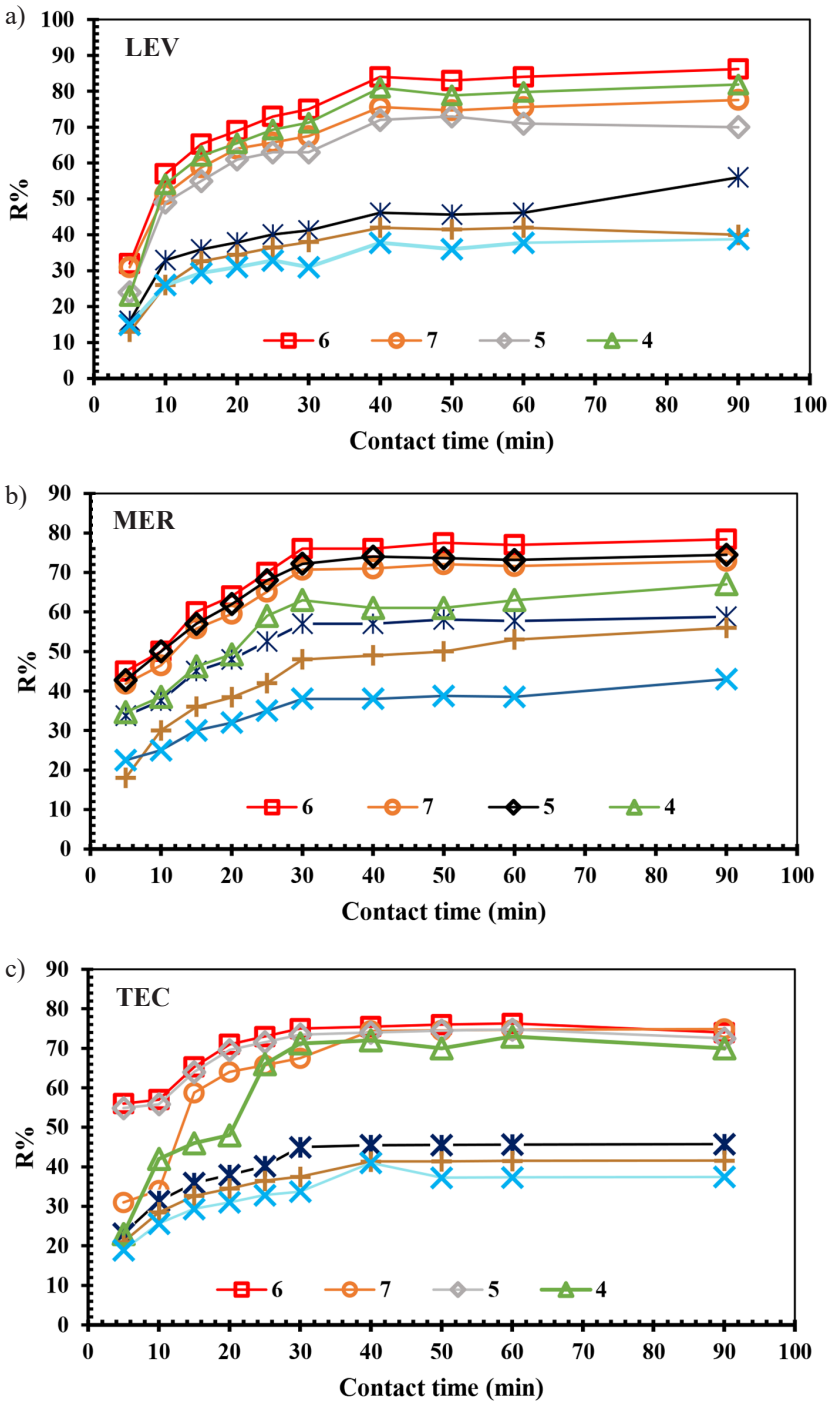

Figure 3. Effect of pH on the LEV, MER, and TEC adsorption efficiency onto CSFH in the ternary system (initial antibiotic concentration = 75 mg/L, temperature = 20 ± 1° C, agitation time from 0 to 90 min at 200 rpm, adsorbent dose = 0.1 g/100 mL)

causing $CuOH_2^+$ groups to form. Ultimately, this positively charges the CuO surface. As the CuO nanoparticles and CSFH have positive net surface charges at pH = 6, electrostatic attraction may occur between them and the negatively charged groups of ternary antibiotics, resulting in strong LEV, MER, and TEC elimination efficiency. However, the adsorption effectiveness decreases when the pH falls below 6, as this causes electrostatic repulsion between positively charged CuO nanoparticles and cationic moieties of ternary antibiotics. The results indicate that adsorption is facilitated whenever the charges of the adsorbents and the LEV, MER, and TEC molecules are dissimilar. This is primarily because electrostatic attraction forces typically emerge when the adsorbate molecules and adsorbent surfaces have different charges. This can result in a chemisorption reaction between the ternary antibiotic molecules and CSFH active sites when pH 6 is reached.

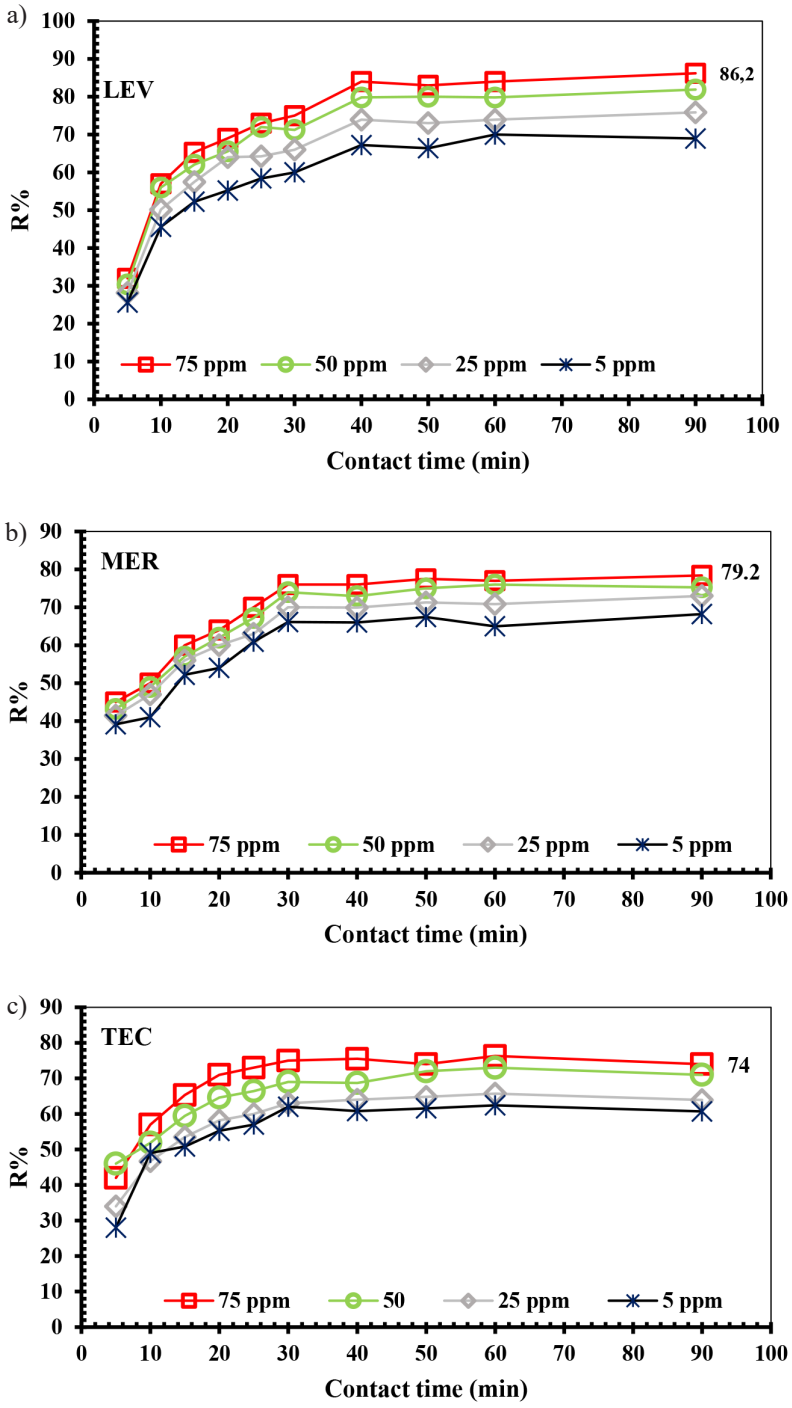

Figure 4. Effect of initial LEV (a), MER (b), and TEC (c) concentrations on their adsorption efficiency in the ternary system

As contact time increases, the elimination efficiencies of the three antibiotics also increase, reaching peak adsorption after approximately 30 min for both MER and TEC and 40 min for LEV (Figure 3). Moreover, the elimination rates for all three antibiotics increased significantly during the first 30 min of contact time, which is most likely caused by the abundance of uncovered adsorption sites on the adsorbent. It is important to note that the rapid removal of the pollutant by the adsorbent is a very beneficial feature and can thus be considered very effective in adsorption treatment processes. However, the removal rate evidently decreases as the contact time progresses between 50 and 90 min. This is most likely due to the continual reduction in available adsorbent reaction sites and concentration of non-adsorbed or non-reacted LEV, MER, and TEC molecules. The removal percentages had been slowly rising until that point. The highest removal efficiencies for LEV (86.2%), MER (78.4%), and TEC (74%) were all reached after a 90-min contact period at pH 6.

Effect of ternary antibiotic concentration

The effects of the LEV, MER, and TEC starting concentrations (5, 25, 50, 75 mg/L for each antibiotic) was examined, as well as their removal percentage by CSFH. These tests were carried out in a controlled setting (pH 6, 20 °C, agitation time 90 min at 200 rpm, adsorbent dose 0.1 g/100 mL). The removal efficiencies of LEV, MER, and TEC increased dramatically as the starting concentration increased (Figure 4). This was caused by the high concentration gradients that emerged at greater adsorbate concentrations (Gupta et al., 2017).

Kinetics of ternary antibiotic adsorption

The kinetic data of LEV, MER, and TEC adsorption onto CSFH were modelled using two kinetic models: pseudo-first-order (Equation 3) and pseudo-second-order (Equation 4). These models are commonly used to model the removal of organic and inorganic pollutants from water solutions. The regression coefficients for each model were calculated through nonlinear fitting procedures in a MATLAB program, with the results being presented in Table 1. The R^2 values show that the pseudo-second-order model is the best-fitting equation for determining the adsorption kinetics of LEV, MER, and TEC onto CSFH. Additionally, a slight difference in the experimental and estimated uptake values was identified in the pseudo-second-order model. This suggests that chemical-based reactions take place between the three antibiotics and CSFH molecules (Aljeboree et al., 2017). Moreover, to explain the intra-particle diffusion mechanisms taking place in the adsorption processes for all three antibiotics, the intra-particle diffusion model (Equation 5) was 3used to evaluate data. This model is frequently employed to ascertain whether intra-particle diffusion or another process (such as film, pore or surface diffusion) is the most significant rate-limiting step (Boparai et al., 2011). The linear trend line fit of q_t versus $t^{0.5}$ point passes very near the point of origin (i.e. the parameter $C \approx 0$). This indicates that intra-particle diffusion is the dominant rate-limiting step in the adsorption kinetic. The intra-particle diffusion equation was thus used to plot the kinetic data of LEV, MER, and TEC adsorption onto CSFH at various initial

Table 1. The kinetic model parameters and regression coefficients for simultaneous levofloxacin (LEV), meropenem (MER), and tetracycline (TEC) adsorption onto CuO coated sunflower husk (CSFH)

Antibiotic	C_0 (mg/L)	q_{exp} (mg/g)	Pseudo-first order			Pseudo-second order			Intra-particle diffusion		
			$q_{cal.}$ (mg/g)	K_1 (min-1)	R^2	$q_{cal.}$ (mg/g)	K_2 (g/mg.min))	R^2	k_{id} (mg/g.min-0.5)	C (mg/g)	R^2
LEV	5	12.24	9.2	0.048	0.94	14.4	0.0049	0.98	1.29	1.85	0.81
	25	26.96	19.3	0.038	0.892	28.8	0.0018	0.99	2.9	1.8	0.86
	50	38.56	12.9	0.032	0.852	41.8	0.0069	0.99	4.1	6.3	0.79
	75	50.48	45.3	0.045	0.981	52.4	0.0021	0.99	5.2	7.3	0.86
MER	5	15.3	20.2	0.056	0.85	12.6	0.0042	0.98	1.5	0.5	0.95
	25	33.7	28	0.047	0.84	35.5	0.0031	0.98	4.1	1.8	0.89
	50	48.2	31.4	0.033	0.82	47.3	0.0024	0.99	3.8	12.5	0.74
	75	63.1	58	0.041	0.89	61.2	0.0013	0.99	5.9	14.9	0.79
TEC	5	8.4	5.3	0.026	0.78	6.4	0.0032	0.94	0.79	1.4	0.96
	25	18.3	9.5	0.029	0.82	15.2	0.0016	0.92	1.8	3.2	0.74
	50	35.8	44	0.035	0.84	33.7	0.0010	0.99	3.4	6.2	0.87
	75	47	41	0.035	0.90	45.9	0.0008	0.97	4.2	12.1	0.72

concentrations. The kinetic data plots produced when the intra-particle diffusion equation is used do not fit the linear equations. Furthermore, the C values are greater than zero. This finding suggests that more than one adsorption mechanism controls the adsorption of LEV, MER, and TEC onto CSFH and that intra-particle diffusion is not the most significant adsorption mechanism.

$$q_t = q_e[1 - exp(-k_1 t)] \quad (3)$$

$$q_t = \frac{k_2 q_e^2 t}{1 + k_2 q_e t} \quad (4)$$

$$q_t = k_{\mathrm{id}} t^{0.5} + C \quad (5)$$

where: q_t (mg/g) – represents the amount of each LEV, MER, and TEC molecule adsorbed onto the CSFH at time t (min);
k_1 and k_2 (min^{-1}) – represent the rate constants of the first- and second-order kinetic models;
k_{id} (mg/g min$^{0.5}$) – is the constant of the intra-particle diffusion rate;
C (mg/g) – represents the constant related to the thickness of the boundary layer.

Isotherms of ternary antibiotic adsorption

The key purpose of studying sorption isotherms is to determine how the sorbed ternary antibiotics are distributed on the solid phase of CSFH compared to the equilibrium of ternary antibiotics concentration in the sorptive phase. The Langmuir (Equation 6) and Freundlich (Equation 7) isotherm models were employed to model the experimental isotherm data for the different adsorbents.

$$q_e = \frac{q_{max} b C_e}{1 + b C_e} \quad (6)$$

$$q_e = K_F C_e^{1/n} \quad (7)$$

$$R_L = \frac{1}{1 + b C_o} \quad (8)$$

where: q_{max} represents the maximum adsorption capacity of the adsorbent (mg/g),
b is a Langmuir constant representing the affinity of the adsorbent's active sites (L/mg), and
n represents the Freundlich constant which pertains to sorption intensity. This equation can be used to determine the desirability of the adsorption process at 1 n < 1. Finally, K_f is the Freundlich constant used to determine the relative sorption capacity (mg/g).

It is interesting to note that the adsorption data for LEV, MER, and TEC fit well in the Langmuir model, whereby suitable correlation coefficient values were identified. These results (Table 2) indicate the existence of a complicated mechanism in which the antibiotics are simultaneously adsorbed onto the CSFH adsorbent's surface consisting of multiple adsorption sites. The Langmuir model analysis showed that the maximum adsorption uptakes were 62.24, 131.83 and 96.95 mg/g for LEV, MER, and TEC, respectively. When Equation (7) was used to determine the values for the best-fit model (represented by n values of LEV and TEC adsorption and the R_L values of MER and TEC), the findings showed that the adsorption process involving the CSFH adsorbent was most effective. The n values were all <1, which suggests that a chemisorption process took place to adsorb all three antibiotics onto the CSFH (Aljeboree et al., 2017). These findings show that CSFH was more efficient in eliminating antibiotic molecules in the adsorption treatment process than other adsorbents were.

Table 2. Calculated isotherm and regression parameters of the LEV, MER, and TEC onto CSFH

Model	Parameter	LEV	MER	TEC
Langmuir	q_{max} (mg/g)	62.24	131.83	96.95
	K_L (L/mg)	0.150	0.047	0.035
	R_L	0.08-0.57	0.22-0.81	0.27-0.85
	R^2	0.973	0.956	0.971
	SD	5.56	8.1	8.0
Freundlich	k_f (mg/g)	12.23	8.41	4.89
	1/n	2.25	1.47	1.44
	R^2	0.949	0.937	0.945
	SD	8.3	8.99	9.5

Thermodynamic properties of ternary antibiotics adsorption

In order to perform a thermodynamic analysis of CSFH for simultaneous LVE, MER, and TEC adsorption, a number of different factors had to be considered, including the thermodynamic parameters of Gibbs free energy change ($\Delta G°$, kJ/mol), surface adsorption of entropy change ($\Delta S°$, kJ/mol.K), and enthalpy change ($\Delta H°$). The solutions containing the three antibiotics were tested at various temperatures between 20 and 40 °C, and the effects of the temperature changes on CSFH elimination efficiency were investigated. The following equations (9–11) was used to calculate the thermodynamic parameters of enthalpy change ($\Delta H°$), entropy change ($\Delta S°$) and Gibbs free energy change ($\Delta G°$).

$$\Delta G^{\circ} = -RT\ln(k_c) \tag{9}$$

$$\Delta G^{\circ} = \Delta H^{\circ} - T\Delta S^{\circ} \tag{10}$$

$$\ln(k_c) = \frac{\Delta S^{\circ}}{R} - \frac{\Delta H^{\circ}}{RT} \tag{11}$$

where: T – refers to the absolute temperature (K);
R – represents the universal gas constant (8.314×10^{-3} kJ mol^{-1} K^{-1});
k_c – (L g^{-1}) represents the thermodynamic distribution coefficient for adsorption.

To calculate k_c, Equation 9 can be applied:

$$k_c = \frac{q_e}{c_e} \tag{12}$$

where: k_c – refers to the different temperatures at equilibrium.

Least square analysis can be performed to identify the linear relationship between ln and 1/T. Additionally, it may also be possible to determine the change in enthalpy that occurs during the adsorbent process at different temperatures.

The data shown in Table 3 reveal that temperature had a minimal impact on the capacity of LEV, MER, and TEC to bind to CSFH. Altogether, there was a minor improvement in the CSFH adsorption capacity, and this is primarily due to a reduction in the viscosity of the solution harbouring the pollutant molecules as the solution temperature rises. In turn, this allows the adsorbate to diffuse at a quicker rate across the bulk (external) and pore (internal) boundaries of the adsorbent particles. Negative ΔG values were identified for all temperatures, and this ultimately indicates that the adsorption reactions between LEV, MER, and TEC molecules and CSFH particles are spontaneous. Nonetheless, negative $\Delta H°$ and ΔS values indicate that the adsorption process was exothermic. Moreover, the level of randomness during the reaction between LEV, MER, and TEC with the CSFH particles was reduced.

ANN prediction model development

The LMA (Levenberg–Marquardt) training algorithm was used in MATLAB to predict the elimination efficiency of ternary antibiotics. The

Table 3. Thermodynamic analysis of the simultaneous adsorption of LEV, MER, and TEC onto CSFH (C_o = 75 mg/L, CSFH dose = 0.1 g/100 mL, agitation time = 90 min at 200 rpm, and pH = 6)

Adsorbate	T (°C)	q_e(mg/g)	Thermodynamic Parameters		
			ΔG°(kJ/mol)	$\Delta H°$(kJ/mol)	$\Delta S°$(kJ/mol.K)
LEV	20	50.48	-1.71	-21.08	-65.77
	25	49.02	-1.57		
	30	46.57	-1.24		
	35	43.31	-0.79		
	40	40.71	-0.45		
MER	20	63.10	-2.79	-13.47	-34.39
	25	61.84	-3.83		
	30	59.36	-3.36		
	35	56.39	-2.84		
	40	53.58	-2.39		
TEC	20	47.00	-1.26	-17.53	-55.45
	25	45.12	-1.02		
	30	42.86	-0.73		
	35	40.72	-0.44		
	40	38.69	-0.16		

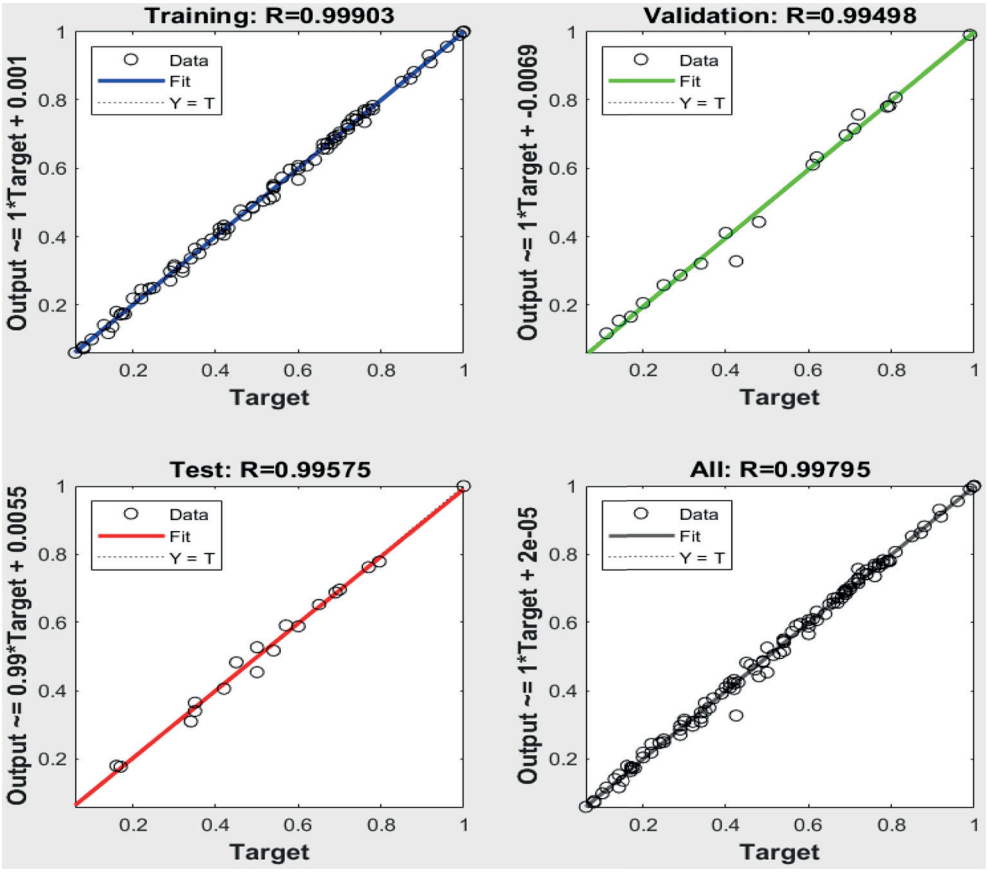

Figure 5. Training, validation and testing regression for the Levenberg-Marquardt algorithm

input adsorption parameters used in the model were as follows: contact time (min.), C_o (mg/L), CSFH Dosage (g/100mL), Temperature (°C), and pH. On the other hand, the efficiency of ternary antibiotic removal (R%) served as the target parameter. Additionally, the mean square error (MSE) was calculated to optimise the NN topology for the prediction and training sets. Figure 5 presents a plot of LMA regression for training, validation, and testing, with all correlation coefficients shown to be in excess of 0.994. On the whole, the newly-developed ANN model is simpler, quicker, and more accurate in calculating the R% than other traditional methods are (Yetilmezsoy and Demirel, 2008).

CONCLUSIONS

In the present study, the capacity of CSFH to adsorb and remove LEV, MER, and TEC from the ternary system was explored. The CSFH adsorbent was characterised by advanced means of TEM, SEM, XRD, and FT-IR. The findings revealed that the prepared adsorbent was generally more effective when the SF was coated in CuO nanoparticles than that without the CuO coating. This improved both the practical utilisation and adsorption capacity. The isotherm analysis showed that heterogeneous and homogeneous adsorption sites were found on the CSFH surface, all of which were ready to react with antibiotic molecules. Moreover, the thermodynamic analysis showed that the adsorption process was both spontaneous and exothermic in nature. The CSFH maximum adsorption capacity for the three antibiotics can be ranked as follows, according to the findings of the Langmuir model: MER > TEC > LEV. The pseudo-second-order model adequately models the kinetic data of the three antibiotics, demonstrating that kinetic adsorption is a chemical-based process. Furthermore, the kinetic investigation revealed that the kinetic rate was controlled by multiple processes. The current study found that CSFH is an excellent adsorbent that can be used to sequester antibiotics in adsorption treatment systems. Finally, the results show that the ANN is an excellent tool for assessing removal efficiency of ternary antibiotics in a wastewater.

Acknowledgements

The authors would like to thank the Universiti Kebangsaan Malaysia (UKM) for financial support under grant DIP-2021-008.

REFERENCES

1. Abed K.M. 2014. Kinetic of Alkaloids Extraction from Plant by Batch Pertraction in Rotating Discs Contactor. Iraqi Journal of Chemical and Petroleum Engineering, 15(2), 75–84.
2. Abed K.M. 2015. Separation of alkaloids from plants by bulk liquid membrane technique using rotating discs contactor: Chemical. Diyala Journal of Engineering Sciences, 8(4), 785–793.
3. Ahmed M.J., Theydan S.K. 2013. Microwave assisted preparation of microporous activated carbon from Siris seed pods for adsorption of metronidazole antibiotic. Chemical Engineering Journal, 214, 310–318.
4. Al-Jabari M.H., Sulaiman S., Ali S., Barakat R., Mubarak A., Khan S.A. 2019. Adsorption study of levofloxacin on reusable magnetic nanoparticles: Kinetics and antibacterial activity. Journal of Molecular liquids, 291, 111249.
5. Aljeboree A.M., Alshirifi A.N., Alkaim A.F. 2017. Kinetics and equilibrium study for the adsorption of textile dyes on coconut shell activated carbon. Arabian Journal of Chemistry, 10, S3381–S3393.
6. Al-Hemiri A.A., Abed K.M., Al-Shahwany A. W. 2012. Extraction of Pelletierine from Punica granatum L. by Liquid Membrane Technique and Modelling. Iraqi Journal of Chemical and Petroleum Engineering, 13(1), 1–9.
7. Attia T.M.S., Hu X.L., Qiang Y.D. 2013. Synthesized magnetic nanoparticles coated zeolite for the adsorption of pharmaceutical compounds from aqueous solution using batch and column studies. Chemosphere, 93(9), 2076–2085.
8. Boparai H.K., Joseph M., O'Carroll D.M. 2011. Carroll Kinetics and thermodynamics of cadmium ion removal by adsorption onto nanozerovalent iron particles. Journal of Hazardous Materials, 186(1), 458–465.
9. Chen, H., Gao, B., Li, H., 2015. Removal of sulfamethoxazole and ciprofloxacin from aqueous solutions by graphene oxide. Journal of Hazardous Materials, 283, 201–207.
10. Danalıoğlu S.T., Bayazit Ş.S., Kuyumcu Ö.K., Abdel Salam M. 2017. Efficient removal of antibiotics by a novel magnetic adsorbent: Magnetic activated carbon/chitosan (MACC) nanocomposite. Journal of Molecular Liquids, 240, 589–596.
11. Dostert K-H., O›Brien C.P., Mirabella F., Ivars-Barceló F., Schauermann S. 2016. Adsorption of acrolein, propanal, and allyl alcohol on Pd(111): a combined infrared reflection–absorption spectroscopy and temperature programmed desorption study. Journal of Physical Chemistry Chemical Physics, 18, 13960–13973.
12. Elragehy N.A., Abdel-Moety E. M., Hassan N.Y., Rezk M.R. 2008. Stability-indicating determination of meropenem in presence of its degradation product. Talanta, 77(1), 28–36.
13. Ersan M., Guler U.A., Acıkel U., Sarioglu M. 2015. Synthesis of hydroxyapatite/clay and hydroxyapatite/pumice composites for tetracycline removal from aqueous solutions. Process Safety and Environmental Protection, 96, 22–32.
14. Figueroa R.A., Leonard A., Mackay A.A. 2004. Modeling tetracycline antibiotic sorption to clays. Environmental Science and Technology, 38(2), 476–483.
15. Fukahori S., Fujiwara T. 2014. Modeling of sulfonamide antibiotic removal by TiO2/high-silica zeolite HSZ-385 composite. Journal of Hazardous Materials, 272, 1–9.
16. Gupta, V.K., Agarwal S., Asif M., Fakhri A., Sadeghi N. 2017. Application of response surface methdology to optimize the adsorption performance of a magnetic graphene oxide nanocomposite adsorbent for removal of methadone from the environment. Journal of Colloid Interface Science, 497, 193–200.
17. Gupta V.K., Saleh T.A. 2013. Sorption of pollutants by porous carbon, carbon nanotubes and fullerene-an overview. Environmental Science and Pollution Research, 20, 2828–2843.
18. Inyang M., Gao B., Zimmerman A., Zhang M., Chen H., 2014. Synthesis, characterization, and dye sorption ability of carbon nanotube-biochar nano composites. Chemical Engineering Journal, 236, 39–46.
19. Mahmoud M.E., El-Ghanam A.M., Mohamed R.H.A., Saad S.R. 2020. Enhanced adsorption of Levofloxacin and Ceftriaxone antibiotics from water by assembled composite of nanotitanium oxide/chitosan/nano-bentonite. Materials Science and Engineering, C, 108, 110199.
20. Michael I., Rizzo L., McArdell C.S., Manaia C.M., Merlin C., Schwartz T., Dagot C., Fatta-Kassinos D. 2013. Urban wastewater treatment plants as hotspots for the release of antibiotics in the environment: A review. Water Research, 47(3), 957–995.
21. Mohammed A.A., Al-Musawi T.J., Kareem S.L. Zarrabi M., Alaa M., Al-Ma'abreh M.A. 2020. Simultaneous adsorption of tetracycline, amoxicillin, and ciprofloxacin by pistachio shell powder coated with zinc oxide nanoparticles. Arabian Journal of Chemistry, 13, 4629–4643.
22. Mohammed S.J., M-Ridha M.J., Abed K.M., Elgharbawy A.A. 2021. Removal of levofloxacin and ciprofloxacin from aqueous solutions and an economic evaluation using the electrocoagulation

process. International Journal of Environmental Analytical Chemistry, 1–19.

23. Mohammed S.J., Mohammed-Ridha M.J. 2021. Optimization of levofloxacin removal from aqueous solution using electrocoagulation process by response surface methodology. Iraqi Journal of Agricultural Sciences, 52(1), 204–217.
24. Mohseni-Bandpi A., Al-Musawi T.J., Ghahramani E., Zarrabi M., Mohebi S., Vahed S.A. 2016. Improvement of zeolite adsorption capacity for cephalexin by coating with magnetic Fe_3O_4 nanoparticles. Journal of Molecular Liquids, 218, 615–624.
25. M-Ridha M.J., Hasan Y.R., Ibrahim M.A. 2020. Adsorption kinetics and mechanisms for meropenem antibiotic removal in batch mode via rice husk functionalized with Mg/Fe-layered double hydroxides. Separation Science and Technology, 56(16), 2721–2733.
26. Pouretedal H.R., Sadegh N. 2014. Effective removal of Amoxicillin, Cephalexin, Tetracycline and Penicillin G from aqueous solutions using activated carbon nanoparticles prepared from vine wood. Journal of Water Process Engineering, 1, 64–73.
27. Ramani R.V., Ramani B.M., Saparia A.D., Dhruv D., Markna J.H. 2015. Synthesis and optical characterization of CuO nanoparticles on solar borosilicate glass. Journal of Nano Research, 37, 68–73.
28. Shaban M.A.A., Ibrahim M.A., M-Ridha M.J., Haitham A. Hussein H.A. 2020. Adsorption of meropenem antibiotics from aqueous solutions on multi-walled carbon nanotube, performance, mechanism, and modeling. International Review of Civil Engineering (I.RE.C.E.), 11(6), 283–293.
29. Shi L., Zhang X., Chen Z. 2011. Removal of chromium (VI) from wastewater using bentonite-supported nanoscale zero-valent iron. Water Research, 45(2), 886–892.
30. Song G., Guoa Y., Lia G., Zhaoc W., Yud Y. 2019. Comparison for adsorption of tetracycline and cefradine using biochar derived from seaweed Sargassum sp. Desalination and Water Treatment, 160, 316–324.
31. Soori M.M., Ghahramani E., Kazemian H., Al-Musawi T.J., Zarrabi M. 2016. Intercalation of tetracycline in nano sheet layered double hydroxide: an insight into UV/VIS spectra analysis. Journal of the Taiwan Institute of Chemical Engineers, 63, 271–285.
32. Sun Y., Li H., Li G., Gao B., Yue Q., Li X. 2016. Characterization and ciprofloxacin adsorption properties of activated carbons prepared from biomass wastes by H_3PO_4 activation. Bioresource Technology, 217, 239–244.
33. Teixeira S., Delerue-Matos C., Santos L. 2019. Application of experimental design methodology to optimize antibiotics removal by walnut shell based activated carbon. Science of the Total Environment, 646, 168–176.
34. Ternes T.A, Joss A., Siegrist H. 2004. Scrutinizing pharmaceuticals and personal care products in wastewater treatment. Environmental Science and Technology, 38(20), 392A–399A.
35. Tian Y., Gao B., Chen H., Wang Y., Li H. 2013a. Interactions between carbon nanotubes and sulfonamide antibiotics in aqueous solutions under various physicochemical conditions. Journal of Environmental Science and Health, 48(9), 1136–1144.
36. Tian Y., Gao B., Morales V.L., Chen H., Wang Y., Li H. 2013b. Removal of sulfa methoxazole and sulfapyridine by carbon nanotubes in fixed-bed columns. Chemosphere, 90(10), 2597–2605.
37. Wang J., Gao B., Dou M., Huang X., Ma Z. 2020. A porous g-C3N4 nanosheets containing nitrogen defects for enhanced photocatalytic removal meropenem: Mechanism, degradation pathway and DFT calculation. Environmental Research, 184, 109339.
38. Wu Q., Li Z., Hong H., Yin K., Tie L. 2010. Adsorption and intercalation of ciprofloxacin on montmorillonite. Applied Clay Science, 50(2), 204–2011.
39. Yang W., Lu Y., Zheng F., Xue X., Li N., Liu, D. 2012. Adsorption behavior and mechanisms of norfloxacin onto porous resins and carbon nanotube. Chemical Engineering Journal, 179, 112–118.
40. Yetilmezsoy K., Demirel S. 2008. Artificial neural network (ANN) approach for modeling of Pb(II) adsorption from aqueous solution by Antep pistachio (Pistacia Vera L.) shells. Journal of Hazardous Materials, 153, 1288–1300.
41. Yi S., Gao B., Sun Y., Wu J., Shi X., Wu B. 2015. Removal of levofloxacin from aqueous solution using rice-husk and wood-chip biochars. Chemosphere, 150, 694–701.